Inlet Distortion Evaluation from Limited High-Response Instrumentation

Stanley H. Ellis*
Pratt & Whitney Aircraft, West Palm Beach, Fla.
and
Barry J. Brownstein†
Air Force Aero Propulsion Laboratory, Dayton, Ohio

Inlet data measured with complete high-response instrumentation are used to establish a new procedure for assessing propulsion system flow stability from tests with limited high-response instrumentation. The most-severe, time-variant inlet distortion levels are predicted within an uncertainty band that is a function of the number of high-response probes and the turbulence level. An appropriate distortion index is used to translate the effects of circumferential and radial distortions into predicted surge margin loss. Substantiating data and a representative stability assessment are presented. This procedure is not accurate enough for stability verification testing. It is intended for use during the early stages of the propulsion system selection and for data validity checks during analysis of time-variant distortion.

Nomenclature

C	= a constant defined by the procedure
δ	= a change in a parameter due to the difference between the most-severe time-variant distortion and the steady-state distortion
$\Delta P/P\square$	= equivalent square-wave pattern intensity
ΔSM	= loss in surge margin due to inlet distortion
ΔSM_{hc}	= loss in surge margin due to hub circumferential distortion[7]
ΔSM_{tc}	= loss in surge margin due to tip circumferential distortion[7]
ΔSM_{hr}	= loss in surge margin due to hub radial distortion[7]
ΔSM_{tr}	= loss in surge margin due to tip radial distortion[7]
$f()$	= a function of the argument enclosed in parentheses
$f(n\text{-probe})$	= dynamic intensification factor (defined in Appendix 5)
K_{a2}	= combined circumferential and radial distortion index[9]
K_{D2}	= circumferential distortion index[8]
K_{ra2}	= radial distortion index[9]
$K\theta$	= circumferential distortion index[1]
MTV	= maximum time-variant
N	= nondimensional index that transforms the average turbulence level into equivalent square-wave pattern intensity
n-probe	= equivalent number of probes averaged in a distortion index
P_{t2}	= average total pressure at the engine-inlet interface
q	= average dynamic head at the compressor inlet
R	= turbulence sampling ratio = (true average turbulence/observed turbulence)
$R_{5\%}$	= 5% of the data are below this value of R
$R_{95\%}$	= 95% of the data are below this value of R
Tu	= turbulence level, $\Delta P_{\text{rms}}/P_{t2}$
$\overline{Tu}$	= face average turbulence, $\Delta P_{\text{rms}}/P_{t2}$

Subscripts

1	= upper boundary of uncertainty band
2	= lower boundary of uncertainty band
c	= circumferential
r	= radial
rms	= root mean square
ss	= steady-state

Introduction

PLOURDE and Brimelow identified a surge-inducing event as the most-severe, time-varant inlet distortion pattern measured with approximately 40 high-response total pressure probes.[1] Because early inlet tests are generally conducted with several low-response probes and only a few high-response probes, a method to estimate distortion levels with this instrumentation will add early compatibility information. The procedure presented in this paper estimates an uncertainty band that is expected to contain the most-severe, time-variant distortion.

Data from four model inlets and two full-scale inlets are used to form correlations between turbulence and maximum time-variant distortion.‡ The general applicability of these correlations is tested by comparison with two additional data sources: another model inlet and a turbulence generator.

Description of the Procedure

The required parameters are: the distortion index formulation, the cutoff frequencies of the compressor and the filter used during inlet tests, the inlet model scale, the steady-state distortion level, the number of high response probes and the observed turbulence. A brief description of the procedure is given below. A flow diagram is shown in Fig. 1. A detailed sample calculation is given in Appendix 3.

The observed turbulence is corrected to the required frequency spectrum and then transformed into an uncertainty band that accounts for sampling error.

Turbulence is transformed into equivalent square-wave patterns. This process further increases the uncertainty band.

Presented as Paper 72-1099 at the AIAA/SAE 8th Propulsion Joint Specialist Conference, November 29–December 1, 1971, New Orleans, La.; submitted April 10, 1973; revision received September 24, 1973. The authors thank the following aircraft companies for permission to use their inlet data: Fairchild Industries, Republic Division; Grumman Aerospace Corporation; McDonnell Douglas Corporation, McDonnell Aircraft; North American Rockwell Corporation, Los Angeles Division.

Index categories: Aircraft Testing (Including Component Aerodynamics); Nonsteady Aerodynamics; Airbreathing Propulsion, Subsonic and Supersonic.

*Senior Project Engineer, Applied Research Dept., Florida Research and Development Center.

†Captain, USAF, Wright Patterson Air Force Base.

‡Additional information qualifying these inlet data is given in Appendix 1.

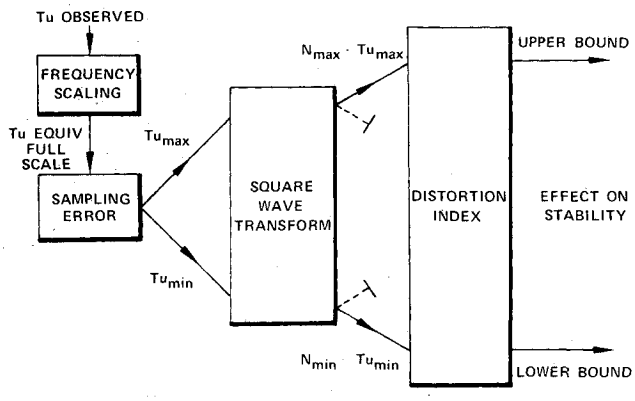

Fig. 1 Flow diagram of procedure.

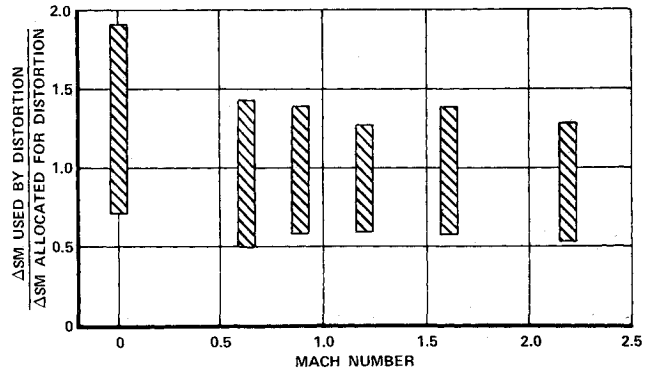

Fig. 2 Inlet/engine compatibility assessment with limited instrumentation.

Equivalent square-wave patterns are transformed into surge margin loss using an appropriate distortion index. Circumferential and radial distortions are combined using the root-sum-square of the individual effects. An additional factor is included in this transformation if the distortion index value is controlled by fewer than 15 probes.§

The surge margin loss due to turbulence is combined with the surge margin loss due to steady-state distortion. For a particular application, the procedure simplifies to

$$\Delta SM = \Delta SM_{ss} + \begin{pmatrix} C_1 Tu \\ C_2 Tu \end{pmatrix} \quad (1)$$

Where C_1 and C_2 define the upper and lower limits of the uncertainty band.

Typical Results

Typical results obtained from tests with limited instrumentation are shown in Fig. 2. The shaded bars in Fig. 2 show a wide range of uncertainty in estimated surge margin loss (the same order as the surge margin allocated for inlet distortion). Only qualitative conclusions can result from the uncertain information shown in Fig. 2; for example, the expected level of inlet distortion is sufficiently close to the allocation to warrant further testing with improved instrumentation.

Although only two high-response probes are used for the stability assessment shown in Fig. 2, the test instrumentation included 40 high-response probes. The most severe distortions measured with the complete, 40 probe instrumentation are compared in Table 1 with estimates based on two probes.

Table 1. Maximum time-variant distortions measured with complete instrumentation compared with estimates based on two high-response probes

	ΔSM Used by distortion / ΔSM Allocated for distortion		
Mach number	Most-severe time-variant distortion	Estimated uncertainty band	Midpoint of uncertainty band
0	0.80	0.72–1.89	1.31
0.6	0.60	0.47–1.42	0.95
0.9	1.12	0.59–1.40	0.99
1.2	0.62	0.59–1.28	0.94
1.6	0.63	0.59–1.39	0.99
2.2	0.64	0.54–1.27	0.90
Maximum value	1.12	0.47–1.89	1.31

§For example, the distortion index [(max-min)/average] is controlled by two probes: the maximum probe and the minimum probe.

All measured time-variant distortions in Table 1 fall within the uncertainty band. This substantiates the procedure because the inlet data and the distortion index used for this typical stability assessment were not used in the procedure formulation. However, these data also show that an inherent lack of precision can result in misleading conclusions if only point estimates are presented. For example, if the stability estimates shown in Table 1 were presented only in terms of the midpoint of each uncertainty band, then two incorrect conclusions may be reached. First, a nonexistent inlet-engine compatibility problem would be indicated at Mach 0; second, a problem at Mach 0.9 would not be disclosed.

Formulation of the Procedure

Turbulence Filtering and Scaling

Pluorde and Brimelow used a low pass analog filter, with a cutoff frequency equal to engine rotor speed, to match time-variant inlet data to the response of a TF30 engine.[1] Turbulence measurements used for stability analysis should also be filtered to match compressor response.

The curve shown in Fig. 3 shows a typical relationship between filter cutoff frequency and the turbulence level generated from a model inlet test at Mach 2.2 and matched ram recovery.[2] Although this relationship changes as the frequency distribution of turbulence changes, the effect is sufficiently small to justify the general use of the curve in Fig. 3 for correcting turbulence to the desired filter frequency.

Model inlets have a different turbulence frequency spectrum than full-scale inlets. Compensation for this difference is made by increasing the filter frequency during model inlet testing. Turbulence data must be translated

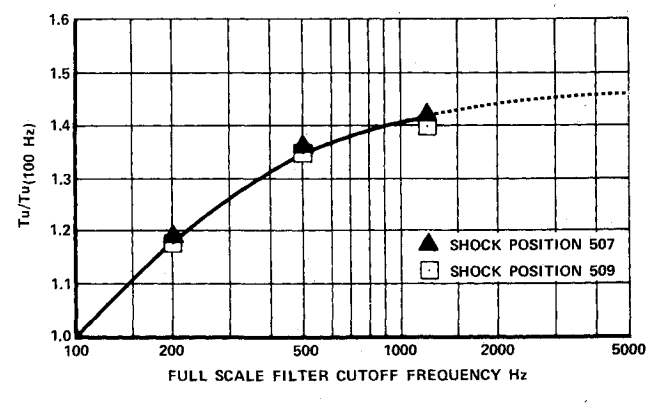

Fig. 3 Correction to turbulence for filter cutoff frequency.

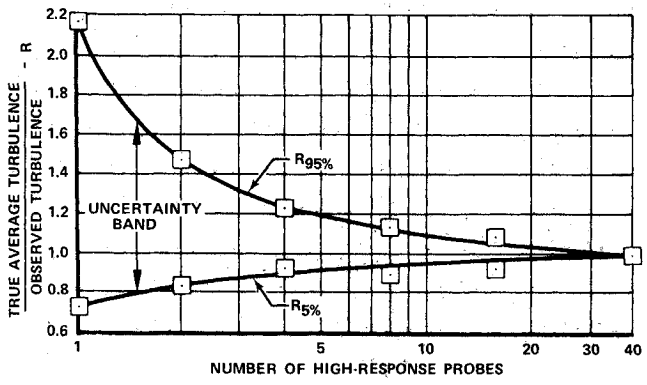

Fig. 4 Turbulence sampling error boundaries.

from the filter frequency used during model tests to that required to match the response of a particular compressor. This translation is accomplished in two steps. First, the cutoff frequency of the filter used during model tests is transformed into an equivalent full-scale frequency; second, the appropriate correction is made to the turbulence level using Fig. 3. The currently accepted procedure to obtain an equivalent full-scale frequency is to multiply the model frequency by the model scale.[2,3] An example showing correction of model inlet turbulence data to a desired compressor response characteristic is given in Appendix 3.

Turbulence Sampling Error

There is considerable turbulence variation across the engine-inlet interface. Consequently, the average turbulence measured by a few high-response probes may not be representative of the average turbulence across the entire interface. This sampling error was investigated using turbulence distribution data from 4 model inlets tested with approximately 40 high-response probes. Probe locations were selected that are typical of current practice: four probes or fewer are assumed to be symmetrically located around the center instrumentation ring only, and 8-, 16-, and 40-probe configurations were assumed to be evenly distributed over the interface area. Upper and lower boundaries of turbulence sampling error, which enclose 90 percent of the data, are shown in Fig. 4 as a function of the number of high-response probes. This relationship is used for transforming an observed value of turbulence into an uncertainty band expected to contain the true face-average turbulence value.

Correlation Between Turbulence and Square-Wave Distortion Patterns

The approach used to relate turbulence level to loss in stability is to translate turbulence into equivalent inlet patterns that have the same effect on compressor stability. These patterns are then translated into surge margin loss using the distortion index for the particular engine or compressor being analyzed. Because most distortion indices are established from tests with simple circumferential and radial square-wave distortion patterns, the intensity of these patterns forms a convenient intermediate description of the effect of turbulence on propulsion-system flow stability.

Both circumferential and radial equivalent square-wave patterns are defined as those patterns giving the greatest loss in surge margin for the particular application. For circumferential distortion, the equivalent pattern produced by turbulence is a square-wave pattern, which is in-phase with the steady-state inlet pattern and has a low-pressure region with an extent that gives the largest loss in surge margin. For radial distortion, the equivalent pressure intensity is either added to or subtracted from the steady-state pressure. An add or subtract decision is made at each radial station to give the greater estimated loss of surge margin.

The turbulence level is transformed into equivalent square-wave pattern intensities using an empirical transformation index N. The equivalent circumferential pattern intensity is defined in terms of [(maximum-minimum)/average] pressure

$$\delta\Delta P/P\square_c = +N\bar{T}u - (-N\bar{T}u) = 2N\bar{T}u \qquad (2)$$

The equivalent radial pattern intensity is defined in terms of [(face average-ring average)/face average] pressure

$$\delta\Delta P/P\square_r = N\bar{T}u \qquad (3)$$

Empirical values of the transform index N were obtained through analysis of time-variant inlet data in terms of the distortion indices K_θ and K_{ra2}. A 180° extent circumferential pattern gives the largest surge margin loss with K_θ. The largest surge margin loss with K_{ra2} is obtained with a radial pattern that moves the combination of the steady-state and equivalent square-wave patterns further from a predetermined base radial profile. For these square-wave patterns the distortion index formulae can be simplified and combined with Eqs. (2) and (3) yielding

For circumferential distortion

$$N\bar{T}u = 0.786\ \delta K_\theta(q/P_{t2}) \qquad (4)$$

For radial distortion

$$N\bar{T}u = \delta K_{ra2}(q/P_{t2}) \qquad (5)$$

Equations 4 and 5 were used to determine values of the transform index, N, shown in Fig. 5. Figure 5 includes data from two full-scale inlets tested at Mach 0 and four model inlets tested over the Mach number range from 0.6 to 2.5.

An appreciable variation in the transform index is noted. This is possibly caused by differences in turbulence distribution and cross correlation. There is no significant difference between the equivalent circumferential and radial distortions produced by turbulence. Also, the variation of the transform index with Mach number is small and ill defined. Therefore, the transformation between turbulence and equivalent pressure patterns is represented by an uncertainty band that applies to both circumferential and radial distortions and is independent of Mach number. The resultant transformation is: for each 1% of

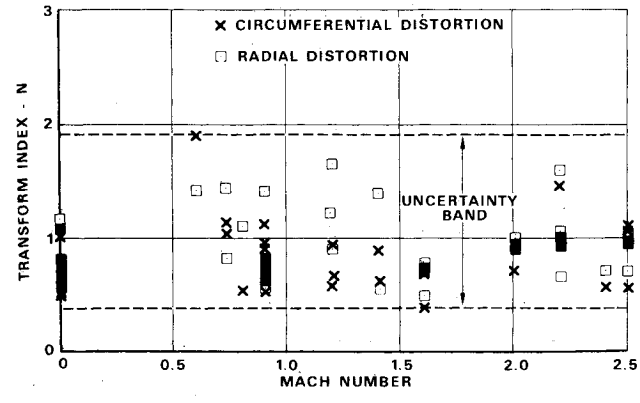

Fig. 5 Correlation between turbulence and square-wave distortion patterns.

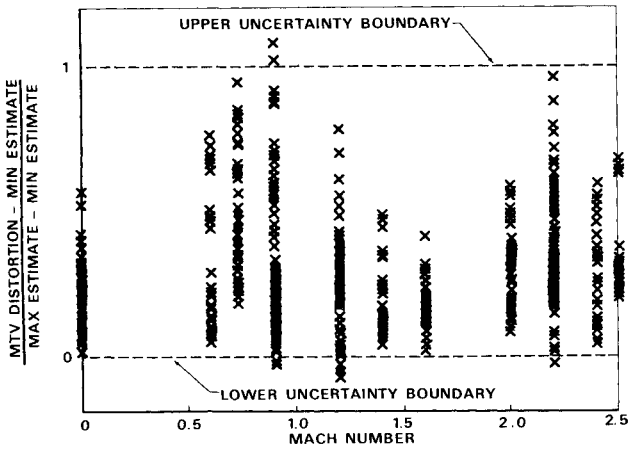

Fig. 6 Substantiation of uncertainty boundaries.

inlet turbulence, the maximum circumferential or radial equivalent square-wave patterns are expected to have intensities between $\pm 0.4\%\ \Delta P/P$ and $\pm 1.9\%\ \Delta P/P$.

Translation to Surge Margin Loss

The effect of circumferential and radial distortions on compressor stability is conveniently described by the appropriate distortion index. All known distortion indices can be translated to the form of Eq. (6) which separates surge margin loss into circumferential and radial elements.

$$\Delta SM = \Delta SM_c + \Delta SM_r \tag{6}$$

Transformation between turbulence and equivalent square-wave patterns yields either the most-severe, circumferential pattern or the most-severe, radial pattern. It is very unlikely that both these patterns exist simultaneously. Because Eq. (6) applies only to superimposed patterns, another method is required for combining the effects of the most-severe circumferential and radial patterns. A statistical approach based on combined normal distributions is discussed below.

The combined distribution of two independent random variables, which have normal probability density functions, can be expressed in terms of a new variable having a mean equal to the sum of the means and a standard deviation equal to the root-sum-square of the individual standard deviations.[4] The difference between steady-state and time-variant circumferential distortion indices approximates a normal distribution with a mean of zero.[5] The corresponding radial distortion distribution has not been investigated; however, it is also expected to be normal because the circumferential and radial data shown on Fig. 5 are similar. A hypothesis for combining circumferential and radial distortions due to turbulence is based on the assumption of independent normal distributions having zero means. This hypothesis is defined by Eq. (7) and is verified if measured, complex, inlet patterns cover the range of the uncertainty boundaries.

$$\delta\Delta SM = (\delta\Delta SM_c^2 + \delta\Delta SM_r^2)^{1/2} \tag{7}$$

Substantiation

Applicable Up to Mach Number 2.5

The most-severe, time-variant pattern of the approximately 1000 inlet patterns analyzed for each data point is compared in Fig. 6 with the upper and lower boundaries of the uncertainty band calculated by this procedure. The

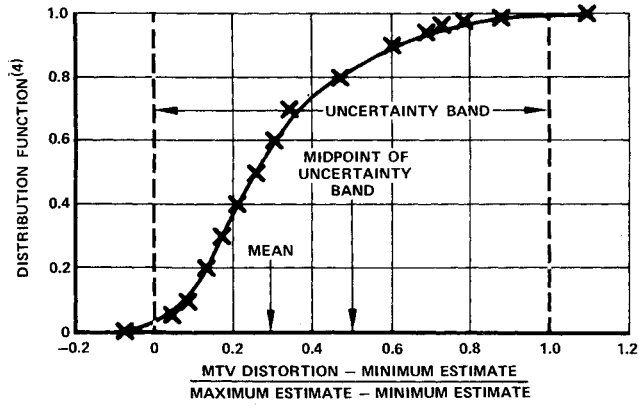

Fig. 7 Data distribution—most of the data are contained within the defined uncertainty band.

data are normalized so that maximum time-variant patterns that produce the same loss in surge margin as the lower and upper boundaries of the uncertainty band are plotted on Fig. 6 at ordinates of 0 and 1.0, respectively. Figure 6 includes 700 data points from 5 model inlets and 2 full-scale inlets. Turbulence data are sampled with two diametrically opposed probes at each of four circumferential locations. Data are analyzed in terms of four circumferential distortion indices, three radial distortion indices, and two indices combining circumferential and radial effects.

It is concluded from Fig. 6 that the procedure is substantially independent of Mach number because the data span the range of the uncertainty band at Mach 0.9 and 2.2. Data at all Mach numbers are, therefore, combined to investigate the effects of other variables.

Data from turbulence generator tests are added to the inlet data shown in Fig. 6 to give the cumulative distribution shown in Fig. 7. The large proportion of data (96%) contained within the uncertainty band in Fig. 7 substantiates the procedure and verifies the hypothesis for combining circumferential and radial distortions due to turbulence.

The skewed distribution of Fig. 7 leads to three possible answers for the best point estimate of the destabilizing effects of turbulence. The maximum limit of the uncertainty band gives the least risk of an undiscovered incompatibility. The mean gives the least mean-square error. The midpoint of the uncertainty band gives the lowest error range. The midpoint and the range of the uncertainty band are recommended for presenting the results of early inlet model tests on a propulsion stability development curve.[6]

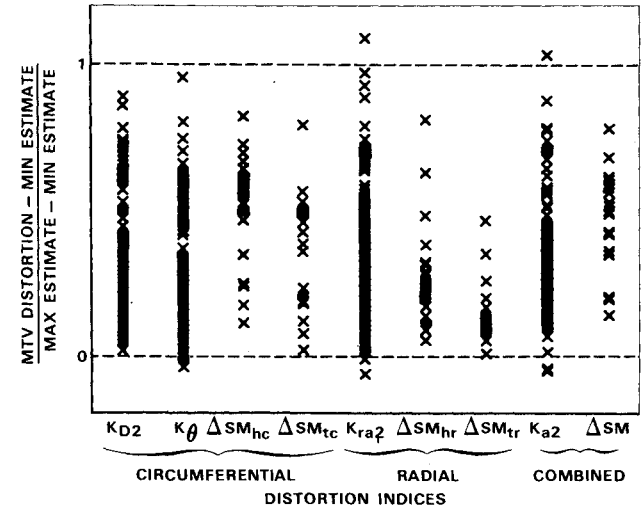

Fig. 8 Procedure applies to several distortion indices.

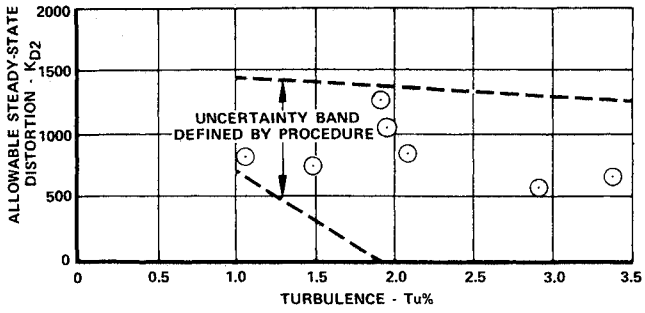

Fig. 9 Comparison with flight data measured with two high-response probes.

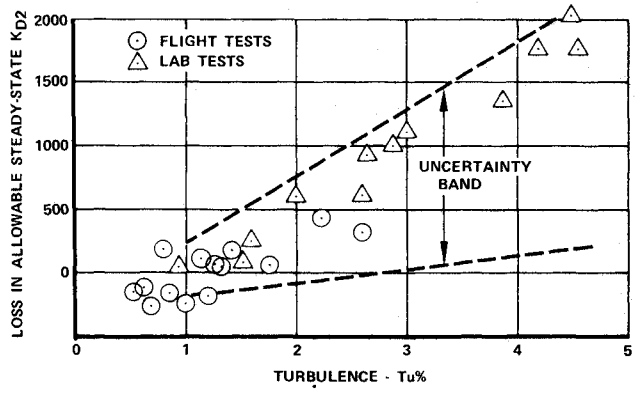

Fig. 10 Comparison with data measured with 40 high-response probes.

Usable With All Distortion Indices

Figure 8 shows the substantiating data sorted into different distortion indices. Because the data scatter is similar, it is concluded that this procedure is applicable to all known distortion indices.

Circumferential distortion indices ΔSM_{hc} and ΔSM_{tc} consider distortions at the hub and tip of the compressor, respectively; these contrast with K_θ, which uses a weighted average of the distortion across the compressor face. These three distortion indices show similar data trends, which suggests that the same relationship between turbulence and an equivalent circumferential pressure pattern holds from hub to tip. Consequently, this procedure is applicable to the stability analysis of the core compressor of a high bypass-ratio engine after appropriate corrections are made for the transfer of distortion across the fan hub.

Applicable to Flight Data

Van Deusen and Mardoc presented TF30/F111 stability data as the loss of allowable steady-state distortion with increasing inlet turbulence.[8]

Most of these data lie within uncertainty boundaries defined by this procedure, as seen in Fig. 9 and 10. This further substantiates the general applicability of this procedure.

Use of the Procedure for Time-Variant Data Validation

Analysis of time-variant distortion requires an automatic data validation procedure because undetected malfunctions—in either the instrumentation or the data reduction equipment—will result in false information processed at a rapid rate.

Continuous monitoring of two parameters is suggested to point out areas where more sophisticated data validity checks are required. The maximum level of time-variant distortion can be continuously updated and compared to the boundaries defined by this procedure. Exceeding the boundaries indicates an error. The average value of time-variant distortion can also be monitored and must be equal to or greater than the steady-state distortion. Failure of this condition also indicates an error.

Summary and Conclusions

A procedure has been established and substantiated to estimate propulsion system flow stability from inlet tests with limited high-response instrumentation. It is applicable to all engines and all inlet data analyzed so far.

The accuracy of estimating surge margin loss is insufficient for stability verification but is adequate for early inlet studies.

This procedure is recommended for assessing flow stability during propulsion system selection and for automatic data validation during analysis of time-variant inlet data.

Appendix 1: Data Base

Data from two-dimensional, external shock inlets were selected at matched ram recovery and the severe angles of attack and sideslip typical of fighter-aircraft operation. Approximately 1000 inlet patterns were defined for each operating condition. These time-variant data were screened to identify the most severe distortion patterns using distortion indices, which represent stability characteristics of several compressors. A total of 48 operating conditions are anlayzed in terms of four existing distortion indices. Six of these are also analyzed in terms of five distortion indices, which are elements of a candidate Universal Distortion Descriptor.

Appendix 2: The Relation Between Distortion Indices and Equivalent Square-Wave Patterns

Most distortion index formulae are simplified by transformation into an equivalent square-wave format. An example of such a transformation is given in Ref. 7. The equivalent square-wave format of several existing distortion indices is given below:

A circumferential 180° square-wave pattern of amplitude $\pm N\,Tu$ gives

$$\delta K_{D2} = 27{,}000 N\bar{T}u \quad \delta K_\theta = 1.27 N\bar{T}u/(1q/P_{t2})$$

A radial square-wave pattern of amplitude $\pm N\ Tu$ gives

$$\delta K_{ra2} = \frac{N\bar{T}u}{q/P_{t2}}$$

The combination of radial and circumferential square-wave patterns, both of amplitude $\pm N\,Tu$, gives

$$\delta K_{a2} = \frac{(1.613 + b^2)^{1/2} N\bar{T}u}{q/P_{t2}}$$

where b is an empirically derived factor for weighting the radial component of distortion.[9]

Appendix 3: Sample Calculations

A sample calculation is presented below. It describes the use of this procedure with a candidate Universal Distortion Descriptor. This distortion descriptor formulation is given in Ref. 7 with an expanded version of this sample calculation.

A 1/7th scale-inlet model is tested at Mach 2.4 with full low-response instrumentation and two high-response probes. Turbulence data are passed through a low-pass fil-

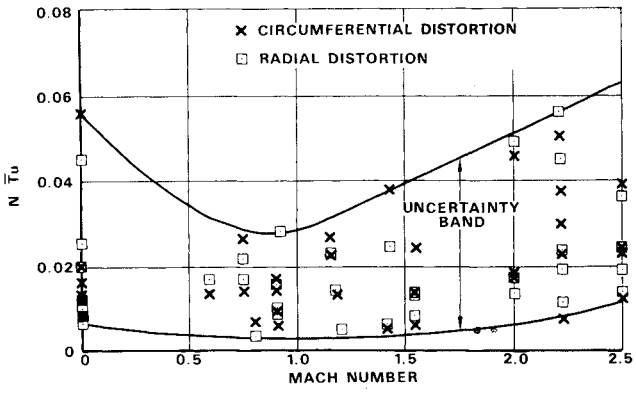

Fig. 11 Equivalent circumferential and radial square-wave patterns due to turbulence.

ter with a cut-off frequency of 4000 Hz; the filter cut-off frequency-matching the compressor response is 200 Hz.

The observed turbulence is: $Tu = 0.023\,\Delta P_{\text{rms}}/P_{t2}$.

The loss in surge margin due to steady-state distortion is: $\Delta SM_{ss} = 0.029$.

1) The equivalent full-scale cutoff frequency corresponding to the filter used in the model tests is the product of the model scale and filter frequency: equivalent full-scale frequency = $(\frac{1}{7})(4000) = 570$ Hz; from Fig. 3: $[Tu_{(570)}/Tu_{(100)}] = 1.37$; entering Fig. 3 at the desired full-scale filter frequency $[Tu_{(200)}/Tu_{(100)}] = 1.19$. The turbulence corrected to 200 Hz is derived by

$$Tu_{(200)} = \frac{Tu_{(200)}/Tu_{(100)}}{Tu_{(570)}/Tu_{(100)}} Tu_{(570)} = \frac{1.19}{1.37} 0.023 = 0.020$$

2) The corrected turbulence is transformed into an uncertainty band to account for sampling error. Entering Fig. 4 at 2 probes: $R_{5\%} = 0.824$, $R_{95\%} = 1.475$.

The upper boundary of interface average turbulence is: $Tu_1 = (1.475)(0.020) = 0.0295$.

The lower boundary of interface average turbulence is: $Tu_2 = (0.824)(0.020) = 0.0165$.

3) The products of the upper and lower turbulence boundaries and the respective uncertainty boundaries of the turbulence transform index shown in Fig. 5 define the over-all upper and lower boundaries of the equivalent square-wave intensities:

Upper boundary of square-wave intensity is: $(N\,Tu)_1 = (1.9)(0.0295) = 0.0561$.

Lower boundary of square-wave intensity is: $(N\,Tu)_2 = (0.40)(0.0165) = 0.0066$.

4) The distortion index formula is changed to a suitable form for transforming equivalent square-wave patterns into the corresponding surge margin loss. If the index is controlled by fewer than 15 probes, the dynamic intensification factor, discussed in Appendix 5, is included in the transformation. The circumferential element of the distortion descriptor is controlled by eight probes. Entering Fig. 12 at eight probes gives a dynamic intensification factor, $f(n\text{-probe})$, of 1.17 for circumferential distortion. The radial element of the distortion descriptor is controlled by 10 probes. Entering Fig. 12 at 10 probes gives a dynamic intensificiation factor of 1.11 for radial distortion. These intensification factors are applied to the distortion correlation developed from tests with square-wave screens to obtain the estimated surge margin loss from the most severe circumferential and radial patterns caused by turbulence.

$$\delta\Delta SM_c = (2N\bar{Tu})(0.49)(1.17) = 1.15N\bar{Tu}$$

$$\delta\Delta SM_r = (N\bar{Tu})(0.51)(1.11) = 0.56\,N\bar{Tu}$$

Where (0.49) and (0.51) are empirical constants defined by the distortion correlations that convert square-wave distortions to surge margin units.

5) Circumferential and radial distortions due to turbulence are now combined using Eq. 7:

$$\delta\Delta SM = N\bar{Tu}(1.15^2 + 0.56^2)^{1/2} = 1.28\,N\bar{Tu}$$

6) The square-wave intensity boundaries defined in step 3 are transformed into surge margin losses using the relationships defined in step 5. These boundaries of dynamic surge margin loss are added to the steady-state value to define an uncertainty band of total surge margin loss.

$$\Delta SM = 0.029 + 1.28\begin{pmatrix}0.056\\0.007\end{pmatrix} = \begin{pmatrix}0.101\\0.038\end{pmatrix}$$

Maximum estimated surge margin loss = 10%
Midpoint surge margin loss = 7%
Minimum estimated surge margin loss = 4%

Appendix 4: Estimating Propulsion System Flow Stability When High-Response Data Are Not Available

Data from five, two-dimensional, external shock inlets are presented in Fig. 11. This curve may be used to provide some assessment of the expected range of maximum time-variant distortion when only low-response data are available. A sample calculation illustrating the use of this curve is given in Ref. 7.

Figure 11 and Eq. 2 show that turbulence can produce a very significant square-wave distortion of 12% (max-min)/av or an insignificant 1%. The wide data scatter emphasizes the need for high-response instrumentation.

Appendix 5: The Effect of Distortion Index Formulation on Dynamic Distortion Measurements

A typical sample of dynamic inlet data is analyzed in Ref. 2 in terms of two simple distortion indices that represent circumferential square-wave patterns. One of these indices is controlled by two probes $(P_{\max} - P_{\min})/P_{\text{av}}$, and the other is controlled by six probes $(P_{\text{high}} - P_{\text{low}})/P_{\text{av}}$. The index controlled by two probe readings gives 60% greater dynamic distortion increment than the index controlled by six probe readings. A similar investigation, undertaken during the formulation of this procedure, is discussed below.

Model inlet data with 40 high-response probes are analyzed in terms of five distortion indices to establish relationships between turbulence and equivalent square-wave inlet patterns, similar to Fig. 5. As expected, the indices controlled by fewer probes indicate higher equivalent square-wave distortion levels than are obtained from the same data analyzed in terms of indices containing more probes. The results of this study are normalized to give the empirical relationship shown in Fig. 12. The ordinate of Fig. 12 is a dynamic intensification factor $f(n\text{-probe})$ which is defined as:

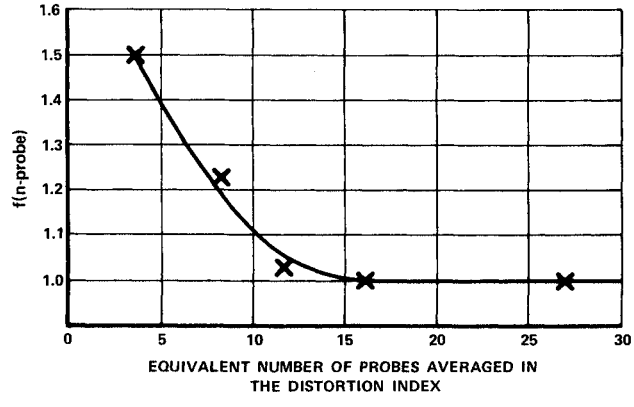

Fig. 12 Dynamic intensification factor.

$$f(n\text{-probe}) = \frac{\left(\begin{array}{c}\text{Equivalent square-wave obtained from dynamic data}\\ \text{by a distortion index controlled by n-probes}\end{array}\right)}{\left(\begin{array}{c}\text{Equivalent square-wave obtained from the same data}\\ \text{by a distortion index controlled by 27 or more probes}\end{array}\right)}$$

The abscissa of Fig. 12 is the equivalent number of probes averaged in the distortion index. The equivalent number of probes is equal to the actual number of probes when probes are equally weighted. For "n" unequally weighted probes with probe "i" having weight W_i, and a maximum probe weight of $W_{\max}$, the equivalent number of probes is defined by Eq. 8.**

$$n\text{-probe} = \frac{\sum_{i=1}^{n} W_i}{W_{\max}} \tag{8}$$

The dynamic intensification factors determined from Fig. 12 were used to modify the steady-state formulae of 9 distortion indices. The resultant stall margin predictions are shown to substantiate this procedure in Fig. 8.

**If the equivalent number of probes is 4, then a change of 1% in the reading of the most heavily weighted probe would produce ¼% change in the distortion index.

References

[1]Plourde, G. A. and Brimelow, B., "Pressure Fluctuations Cause Compressor Instability," *Airframe/Propulsion Compatibility Symposium,* AFAPL-TR-69-103, Air Force Aero Propulsion Lab., Air Force Flight Dynamics Lab., Wright-Patterson Air Force Base, Ohio, June 1969, pp. 567–603.

[2]Beaulieu, W. D., Boyd, H. E., Jr., Kostin, L. C., and Martin, A. W., "Propulsion System Flow Stability Program (Dynamic) Phase II, Part VI Inlet Turbulence Scaling," AFAPL-TR-69-113, Pt. VI, Feb. 1970, Air Force Aero Propulsion Lab., Wright-Patterson Air Force Base, Ohio.

[3]Oates, G. C., Sherman, D. A., and Motycka, D. L., "Experimental Study of Inlet-Generated Pressure Fluctuations," *Airframe/Propulsion Compatibility Symposium,* AFAPL-TR-69-103 Air Force Aero Propulsion Lab., Air Force Flight Dynamics Lab., Wright-Patterson Air Force Base, Ohio, June 1969, pp. 427–457.

[4]Hogg, R. V. and Craig, A. T., "Distributions of Random Variables," *Introduction to Mathematical Statistics,* 3rd ed., MacMillan Company, Collier-McMillan, Limited, London, 1970, pp. 157–159.

[5]Johnson, R. H., Bayati, J. E., Lum, E. L., and Martin, A. W., "Compressor Stability Assessment Program, Air Induction System Considerations," AFAPL-TR-72-30, Aug. 1972, Air Force Aero Propulsion Lab., Wright-Patterson Air Force Base, Ohio.

[6]Brimelow, R., "Techniques for Establishing Propulsion System Stability," APTA TM-69-12, April 1969, Air Force Aero Propulsion Lab., Air Force Systems Command, Wright-Patterson Air Force Base.

[7]Ellis, S. H. and Brownstein, B. J., "A Procedure For Estimating Maximum Time-Variant Distortion Levels With Limited Instrumentation," AIAA Paper 72-1099, New Orleans, La., 1972.

[8]Van Deusen, E. A. and Mardoc, V. R., "Distortion and Turbulence Interaction, A Method for Evaluating Engine/Inlet Compatibility," AIAA Paper 70-632, San Diego, Calif., 1970.

[9]Crites, R. C., "The Philosophy of Analog Techniques Applied to the Analysis and High Speed Screening of Dynamic Data," AIAA Paper 70-595, Tullahoma, Tenn., 1970.